THE JOURNAL OF BIOLOGICAL CHEMISTRY VOL. 283, NO. 47, pp. 32317–32327, November 21, 2008

An Unusual RNA Recognition Motif Acts as a Scaffold for Multiple Proteins in the Pre-mRNA Retention and Splicing Complex*

Received for publication, June 30, 2008, and in revised form, September 8, 2008 Published, JBC Papers in Press, September 22, 2008, DOI 10.1074/jbc.M804977200

Simon Trowitzsch[‡§], **Gert Weber**[‡§], **Reinhard Lührmann**[‡], **and Markus C. Wahl**[§¶1]

From [‡]*Zelluläre Biochemie and* [§]*Makromolekulare Röntgenkristallographie, Max-Planck-Institut für Biophysikalische Chemie, Am Fassberg 11, D-37077 Göttingen, Germany and* [¶]*Röntgenkristallographie, Universitätsmedizin Georg-August-Universität Göttingen, Justus-von-Liebig-Weg 11, D-37077 Göttingen, Germany*

The yeast pre-mRNA retention and splicing complex counteracts the escape of unspliced pre-mRNAs from the nucleus and activates splicing of a subset of Mer1p-dependent genes. A homologous complex is present in activated human spliceosomes. In many components of the spliceosome, RNA recognition motifs (RRMs) serve as versatile protein-RNA or protein-protein interaction platforms. Here, we show that in the retention and splicing complex, an atypical RRM of the Snu17p (small nuclear ribonucleoprotein-associated protein 17) subunit acts as a scaffold that organizes the other two constituents, Bud13p (bud site selection 13) and Pml1p (pre-mRNA leakage 1). GST pull-down experiments and size exclusion chromatography revealed that Snu17p constitutes the central platform of the complex, whereas Bud13p and Pml1p do not interact with each other. Fluorimetric structure probing showed the entire Bud13p and the N-terminal third of Pml1p to be natively disordered in isolation. Mutational analysis and tryptophan fluorescence confirmed that a conserved tryptophan-containing motif in the C terminus of Bud13p binds to the core RRM of Snu17p, whereas a different interaction surface encompassing a C-terminal extension of the Snu17p RRM is required to bind an N-terminal peptide of Pml1p. Isothermal titration calorimetry revealed 1:1 interaction stoichiometries, large negative binding entropies, and dissociation constants in the low nanomolar and micromolar ranges for the Snu17p-Bud13p and the Snu17p-Pml1p interactions, respectively. Our results demonstrate that the noncanonical Snu17p RRM concomitantly binds multiple ligand proteins via short, intrinsically unstructured peptide epitopes and thereby acts as a platform that displays functional modules of the ligands, such as a forkhead-associated domain of Pml1p and a conserved polylysine motif of Bud13p.

The expression of most eukaryotic protein-encoding genes involves precursor messenger RNA (pre-mRNA)[2] processing steps, including pre-mRNA splicing. During pre-mRNA splicing, a multisubunit RNA-protein enzyme, the spliceosome, carries out two successive transesterification reactions that lead to the removal of noncoding intervening sequences (introns) and the concomitant ligation of coding regions (exons). A functional spliceosome emerges from the stepwise recruitment of small nuclear ribonucleoprotein particles (snRNPs) and numerous non-snRNP proteins to the pre-mRNA substrate and subsequent major conformational and compositional rearrangements, which bring about a catalytically competent particle (reviewed in Refs. 1–4). During assembly, the spliceosome traverses distinct maturation and catalysis intermediates.

Several snRNP-associated as well as non-snRNP splice factors are preorganized as multimeric functional modules. For example, the 17 S U2 snRNP encompasses the complex splice factors SF3a and SF3b (splicing factor 3a and 3b, respectively) (5), which harbor three and seven subunits in humans, respectively (6, 7). Similarly, the non-snRNP CDC5 (cell division control protein 5)-Prp19p (pre-mRNA processing factor 19) complex comprises six core components that concomitantly join the spliceosome just prior to catalytic activation (8–11). Recently, a novel ternary non-snRNP protein complex that proved to be important for the retention of unspliced pre-mRNAs in the nucleus has been identified in *Saccharomyces cerevisiae* (12). Since the complex additionally enhanced splicing of a subset of pre-mRNAs, it was termed pre-mRNA *re*tention and *s*plicing complex, RES (12).

The yeast RES complex consists of three proteins, Snu17p (small nuclear ribonucleoprotein-associated protein 17), Bud13p (bud site selection 13), and Pml1p (pre-mRNA leakage 1) (12). Component analyses of isolated human A and B spliceosomal complexes showed that putative human orthologs of the three subunits are present in purified B but not in A complexes, in line with the overall dramatic compositional differences of these two spliceosomal states (13, 14). Consistent with its presence in B complex spliceosomes, it has been shown that the RES complex elicits effects on splicing prior to the first transesterification step in yeast (12, 15). The human RES complex remains associated with the spliceosome after the first transesterification step (C complex), and the ortholog of Bud13p becomes stably incorporated into its catalytic core (16).

* This work was supported by the Max-Planck-Society (to R. L. and M. C. W.). The costs of publication of this article were defrayed in part by the payment of page charges. This article must therefore be hereby marked "*advertisement*" in accordance with 18 U.S.C. Section 1734 solely to indicate this fact.

[1] To whom correspondence should be addressed: Zelluläre Biochemie/Makromolekulare Röntgenkristallographie, Max-Planck-Institut für Biophysikalische Chemie, Am Fassberg 11, D-37077 Göttingen, Germany. Tel.: 49-551-201-1046; Fax: 49-551-201-1197; E-mail: mwahl@gwdg.de.

[2] The abbreviations used are: pre-mRNA, precursor messenger RNA; FHA, forkhead-associated; GST, glutathione *S*-transferase; ITC, isothermal titration calorimetry; RES, pre-mRNA retention and splicing complex; RRM, RNA recognition motif; snRNP, small nuclear ribonucleoprotein particle; UHM, U2AF homology motif; ULM, UHM ligand motif.

Evidently, pre-mRNA splicing critically hinges both on durable as well as on dynamic interactions among spliceosomal proteins and RNAs. One of the most widespread interaction devices in spliceosomal proteins is the RNA recognition motif (RRM). Classical RRMs are 80–90-residue domains, comprising a four-stranded antiparallel β-sheet backed by two α-helices (helices A and B) on one side (17). They serve as RNA-binding elements, often employing two conserved sequence motifs, RNP1 and RNP2, located on the central two β-strands to engage in RNA contacts (18). More recently, a number of proteins have been described, in which RRMs mediate protein-protein interactions. For example, U2AF (U2 auxiliary factor) homology motifs (UHMs) comprise a family of atypical RRMs, which interact with peptide ligands termed UHM-ligand motifs (ULMs) (19).

We have set out to elucidate the molecular architecture of the RES complex. We find that the complex is organized around an unconventional RRM in Snu17p that provides two separate interaction surfaces, to which Bud13p and Pml1p bind at the same time. The two interaction modes sustained by Snu17p resemble binding strategies that have previously been observed separately in RRM-protein complexes; the Snu17p-Bud13p interaction exhibits characteristics of a UHM·ULM complex, whereas the Snu17p-Pml1p interaction is reminiscent of the complex between the SF3b14a (p14) and SF3b155 (splicing factor 3b 155-kDa subunit) proteins (20, 21). We suggest that by binding to short, intrinsically unstructured regions in Bud13p and Pml1p, Snu17p acts as a showcase for other conserved, functional portions of the ligand proteins.

EXPERIMENTAL PROCEDURES

General Cloning Strategies—For cloning of the genes YIR005w, YGL174w, and YLR016c, coding for Snu17p, Bud13p, and Pml1p, respectively, chromosomal DNA was isolated from *Saccharomyces cerevisiae* by standard techniques. Coding sequences were amplified by PCR and cloned into pGEX-6P-1 (GE Healthcare). All constructs were verified by DNA sequencing. Other constructs encoding portions of Snu17p, Bud13p, and Pml1p were amplified from the respective full-length genes, cloned by similar strategies, and also verified by DNA sequencing. For GST pull-down and isothermal titration calorimetry (ITC) experiments, gene fragments coding for Snu17p-(1–148), Snu17p-(9–148), Snu17p-(25–148), Snu17p-(1–138), Snu17p-(9–138), Snu17p-(25–138), Snu17p-(1–125), Snu17p-(9–125), Snu17p-(25–125), Snu17p-(1–106), Snu17p-(9–106), Snu17p-(25–106), Bud13p-(1–64), Bud13p-(1–96), Bud13p-(1–127), Bud13p-(1–162), Bud13p-(1–266), Bud13p-(34–266), Bud13p-(65–266), Bud13p-(97–266), Bud13p-(128–266), Bud13p-(163–266), Bud13p-(202–266), Pml1p-(1–61), Pml1p-(1–89), Pml1p-(1–112), Pml1p-(1–136), Pml1p-(1–161), Pml1p-(1–204), Pml1p-(34–204), Pml1p-(62–204), Pml1p-(90–204), and Pml1p-(113–204) were cloned into the pETM-10 vector (European Molecular Biology Laboratory) that allows the generation of His_6-tagged fusion proteins. For co-expression experiments, full-length genes coding for Snu17p, Bud13p, and Pml1p were cloned into the Duet vector series (pRSFDuet-1, pETDuet-1, pCDFDuet-1, respectively; Novagen). An N-terminal His_6-tag was engineered on Snu17p.

GST Pull-down Assays and Size Exclusion Chromatography—GST fusions of Snu17p, Bud13p, Pml1p, and GST alone were expressed in *Escherichia coli* Rosetta2 (DE3) cells (Novagen) from the respective pGEX-6P-1 plasmids and His_6-tagged polypeptides of Snu17p, Bud13p, and Pml1p were expressed from pETM-10 vectors. GST and the GST fusion proteins were captured on glutathione-coated Sepharose beads (GE Healthcare) and washed extensively with buffer A (50 mM Tris-HCl, pH 7.5, 300 mM NaCl, and 1 mM dithiothreitol). His_6-tagged fragments were prepurified via Ni^{2+}-nitrilotriacetic acid-agarose (Qiagen) and eluted in buffer A supplemented with 300 mM imidazole. 20 μl of protein-coated glutathione-beads were used per binding reaction and incubated with an excess of the respective His_6-tagged protein for 2 h on ice. After extensive washing with buffer B (50 mM Tris-HCl, pH 7.5, 250 mM NaCl, 1 mM dithiothreitol), proteins were eluted by the addition of SDS sample buffer, and half of the fractions were analyzed by SDS-PAGE.

For analytical size exclusion chromatography, His_6-tagged Snu17p, Pml1p, and Bud13p proteins were mixed in approximately equimolar ratios, applied on a Superdex-200 PC 3.2 column (GE Healthcare), and chromatographed in 50 mM Tris-HCl, pH 7.5, 150 mM NaCl, 1 mM dithiothreitol using a SMART protein purification system (GE Healthcare). For a typical run, 50 μl of sample were loaded on the column at a flow rate of 40 μl/min. 40-μl fractions were collected and analyzed by SDS-PAGE.

Mutational Analysis of the Snu17p-Bud13p Complex—A W232A point mutation was introduced into His_6-tagged Bud13p-(202–266) by using the QuikChange site-directed mutagenesis kit (Stratagene) and confirmed by sequencing. Wild type and mutant fragments were produced in *E. coli* and purified via Ni^{2+}-nitrilotriacetic acid resin. A 3-fold molar excess of either His_6-tagged Bud13p-(202–266) or Bud13p-(202–266) (W232A) were incubated with His_6-tagged Snu17p for 3 h at 4 °C. 50 μl of the protein mix was applied on a Superdex-75 PC 3.2 column and chromatographed using the SMART protein purification system (GE Healthcare) at a flow rate of 40 μl/min. 40-μl fractions were collected and analyzed by SDS-PAGE.

Isothermal Titration Calorimetry—His_6-tagged proteins were expressed, captured on Ni^{2+}-nitrilotriacetic acid resin, washed, and eluted as above. All proteins were further purified via gel filtration on a Superdex-75 26/60 column (GE Healthcare) in buffer C (10 mM sodium/potassium phosphate, pH 7.5, 150 mM NaCl, 1 mM β-mercaptoethanol). An additional ion exchange chromatographic step via CM-Sepharose was required to remove residual impurities from Pml1p-(1–204) and Bud13p-(1–266). All purified samples were dialyzed twice against the same batch of buffer C overnight. SDS-PAGE analysis suggested purities above 95% for each polypeptide. All protein concentrations were determined based on the absorbance at 280 nm using calculated extinction coefficients.

The thermodynamics of binding of His_6-tagged full-length proteins and minimal fragments of Bud13p and Pml1p (Bud13p-(1–266), Bud13p-(202–266), Bud13p-(202–266) (W232A), Pml1p-(1–204), and Pml1p-(1–61); employed as titrants) to His_6-tagged full-length or minimal fragments of

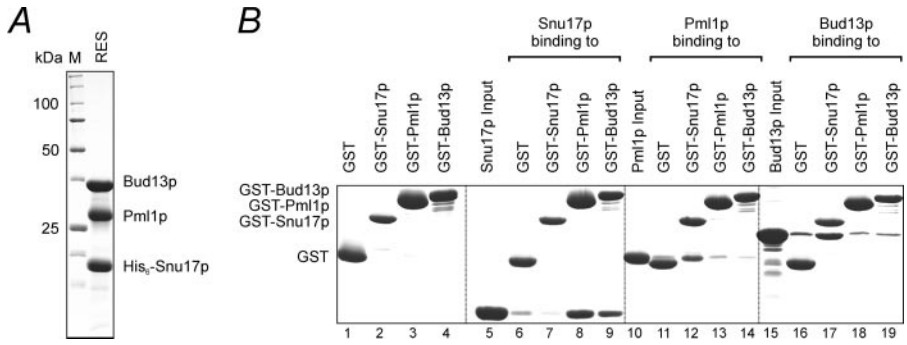

FIGURE 1. ***In vitro* reconstitution of the RES complex.** *A*, SDS-PAGE analysis of purified recombinant RES complex from co-expressed components. Proteins are identified on the *right*. *B*, GST pull-down assays. GST fusion proteins of Snu17p, Pml1p, and Bud13p were produced in *E. coli* and bound to glutathione-Sepharose beads. Prepurified His_6-tagged Snu17p and Bud13p and untagged Pml1p were mixed with GST fusion protein-coated glutathione-Sepharose, and protein fractions bound to the beads were analyzed by SDS-PAGE. *Lanes 1–4* represent the bait input controls. *Lanes 5*, *10*, and *15* are input controls for the His_6-tagged proteins Snu17p, Pml1p, and Bud13p, respectively, used as preys. *Lanes 6*, *11*, and *16* show controls with GST alone, *lanes 7*, *12*, and *17*; *lanes 8*, *13*, and *18*; and *lanes 9*, *14*, and *19* show pull-downs with GST-Snu17p, GST-Pml1p, and GST-Bud13p, respectively, used as baits.

Snu17p (Snu17p-(1–148), Snu17p-(25–138), and Snu17p-(25–106); employed as analytes) were determined using a VP-ITC microcalorimeter (MicroCal Inc.). A typical experiment involved 60 μM titrant in a 300-μl injection syringe and 1300 μl of analyte at 6 μM in the sample cell. ITC analyses were carried out at 20 °C with 20 injections of 15 μl at 5-min intervals. Plain buffer was injected into protein solutions as a control. The heat releases from the control experiments were subtracted from the experimental data before evaluation. Data were analyzed with Microcal Origin 7.0 to extract the enthalpies and entropies of binding (ΔH_a and ΔS_a, respectively), the equilibrium dissociation constants (K_d), and the interaction stoichiometries (n; Table 1).

Fluorescence-based Analysis of Thermal Protein Unfolding—His_6-tagged, purified proteins Snu17p-(1–148), Pml1p-(1–204), and Bud13p-(1–266) were diluted in buffer (20 mM sodium/potassium phosphate, 200 mM NaCl, 0.5 mM dithiothreitol, pH 7.5) to a final concentration of 30 μM. 40-μl reaction volumes were transferred to a 96-well plate. After applying 4 μl of the fluorophore SYPRO Orange (Invitrogen) to each reaction, the change in fluorescence emission upon increasing the temperature in 1 °C steps was monitored on a DNA Engine Opticon™ (MJ Research). The starting temperature was set to 15 °C, and the final temperature was set to 95 °C. Equilibration was for 30 s after temperature ramps. Fluorescence intensities were plotted as a function of temperature and corrected for the signal of the dye in buffer.

CD Spectroscopy—His_6-tagged fragments Snu17p-(25–138), Pml1p-(1–61), and Bud13p-(202–266) were obtained as described above but were further purified via a Superdex-75 gel filtration (GE Healthcare). Measurements were performed on a Chirascan Circular Dichroism Spectrometer (Applied Photophysics). Polypeptides were dissolved in buffer D (10 mM sodium/potassium phosphate, 150 mM NaF, pH 7.9). Measurements were performed at 20 °C with polypeptide concentrations of 25 μM. Data were corrected for the buffer signal and analyzed using the manufacturer's software.

RESULTS

In Vitro Reconstitution of the RES Complex—Tandem affinity purification has revealed that proteins Snu17p, Bud13p, and Pml1p form the RES complex in yeast (12). To test whether recombinant RES components also assemble *in vitro*, we cloned the genes encoding the three proteins from yeast chromosomal DNA. When co-expressed in *E. coli*, the recombinant proteins could be purified as a stable, ternary complex using affinity chromatography and gel filtration (Fig. 1*A*). Significantly, a stable complex could also be reconstituted by mixing components that were expressed and purified individually. Both the co-expressed and the *in vitro* reconstituted particles were stable in the presence of high salt (up to 800 mM NaCl) during gel filtration, suggesting that the interactions between the components involve hydrophobic contacts. Complexes obtained by either strategy migrated similarly in size exclusion chromatography and appeared stoichiometric on SDS gels (Fig. 2). The complexes, therefore, seem to be identical, containing one copy of each subunit. The spontaneous and specific association of the components suggests that these complexes are also identical to the original, tandem affinity purification-purified complex. The ability to reconstitute the ternary complex from isolated components enabled us to derive a detailed interaction map.

Snu17p Is the Central Component of the RES Complex—To elucidate which components of the RES complex directly interact with each other, we performed GST pull-down experiments employing full-length Snu17p, Bud13p, and Pml1p. Immobilized GST-Snu17p brought down both Bud13p and Pml1p (Fig. 1*B*, *lanes 12* and *17*), whereas GST-Bud13p and GST-Pml1p only interacted with Snu17p (Fig. 1*B*, *lanes 8* and *9*). No interaction was observed between Bud13p and Pml1p (Fig. 1*B*, *lanes 14* and *18*). To confirm this molecular organization, we analyzed pairwise combinations of the proteins by size exclusion chromatography. Snu17p formed heterodimers with either Bud13p or Pml1p, which were stable during gel filtration even in the absence of the respective third component (Fig. 2, *D* and *E*). Consistent with the GST pull-down experiments, we were not able to isolate a stable Bud13p-Pml1p heterodimer (Fig. 2*F*).

Domain Organization of the RES Proteins—In order to define interacting domains of the protein, we first analyzed their intrinsic structural organizations. Primary sequence analysis indicated the presence of a RRM in the center of Snu17p and of a forkhead-associated (FHA) domain in the C-terminal part of Pml1p, whereas no known folding unit was detected in the Bud13p sequence (12). Instead, Bud13p appeared to belong to the group of intrinsically unstructured proteins. Consistent with this analysis, Snu17p (17.1 kDa) and Pml1p (23.7 kDa) eluted at the expected retention volumes for approximately

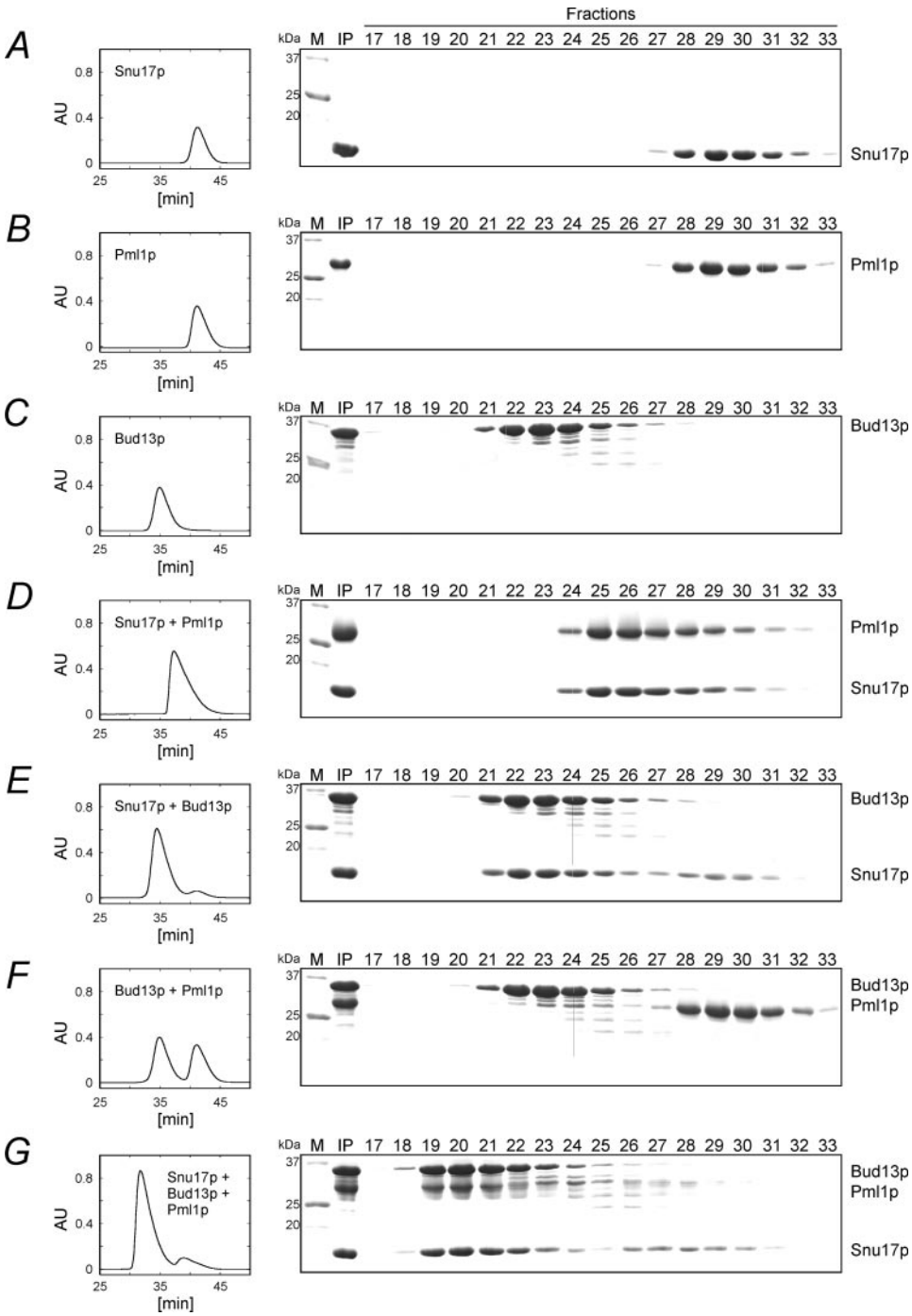

FIGURE 2. **Interaction mapping by gel filtration.** Analysis of RES complex assembly by analytical size exclusion chromatography reveals that Snu17p provides a binding platform for Pml1p and Bud13p. *Left*, elution profiles. *Right*, SDS gel analysis of the elutions. *A–C*, gel filtration analyses of isolated His_6-tagged Snu17p (*A*), Pml1p (*B*), and Bud13p (*C*). *D–F*, gel filtration analyses of two-component mixtures Snu17p + Pml1p (*D*), Snu17p + Bud13p (*E*), and Bud13p + Pml1p (*F*). *G*, gel filtration analysis of the fully assembled RES complex. *AU*, absorption units at 280 nm.

globular proteins in analytical gel filtration runs (Fig. 2, *A* and *B*). In contrast, Bud13p (30.5 kDa) showed an abnormal migration behavior (Fig. 2*C*).

Stable three-dimensional folds in proteins exhibit cooperative unfolding upon increase in temperature or denaturant concentration. As an experimental test for the presence of folded domains, we monitored thermal melting of the three proteins using a fluorescence-based assay (22). Consistent with the fold prediction, Snu17p and Pml1p underwent cooperative unfolding (Fig. 3*A*, *solid* and *dashed black lines*, respectively). No such transition could be discerned with Bud13p (Fig. 3*A*, *gray line*), verifying that this protein lacked regular tertiary structure in isolation.

Minimal Regions of Snu17p Required for Binding of Bud13p and Pml1p—Disorder predictions (23) showed that the central RRM of Snu17p (residues 25–106) is flanked by putatively unstructured regions. To delineate the minimal regions of Snu17p sufficient for binding of Bud13p and Pml1p, we generated His_6-tagged N- and C-terminal truncation mutants of Snu17p (Fig. 4*A*). None of the deletions corrupted the predicted core RRM. We then performed GST pull-down experiments with GST-tagged Bud13p and Pml1p. N-terminal truncations of Snu17p (Snu17p-(9–148) and Snu17p-(25–148)) maintained binding to both Bud13p and Pml1p (Fig. 4, *B* and *C*, *lanes 8* and *11*, respectively). Similarly, short truncations from the C terminus of Snu17p (Snu17p-(1–138), Snu17p-(1–125), and Snu17p-(1–106)) did not affect the binding to Bud13p (Fig. 4*B*, *lanes 14*, *23*, and *32*). In sharp contrast, deletion of more than 10 residues from the C terminus of Snu17p (Snu17p-(1–125) and Snu17p-(1–106)) completely abolished the binding to Pml1p (Fig. 4*C*, *lanes 23* and *32*). These data demonstrate that the core RRM of Snu17p (Snu17p-(25–106)) is sufficient to form a complex with Bud13p but that a C-terminal expansion beyond the core RRM (Snu17p-(25–138)) is required for Pml1p binding.

A Conserved C-Terminal Motif of Bud13p Interacts with Snu17p—Multiple sequence alignments of Bud13p orthologs revealed two highly conserved regions (Fig. 5*A*) (12). The first, at the very N terminus of the protein, contains a high fraction of lysine residues. The second region comprises about 20 residues close to the C terminus (Fig. 5*A*). We asked whether either of the conserved regions in Bud13p constituted an interaction element for Snu17p. Various N- and C-terminally truncated fragments of Bud13p were generated and inspected for binding to immobilized

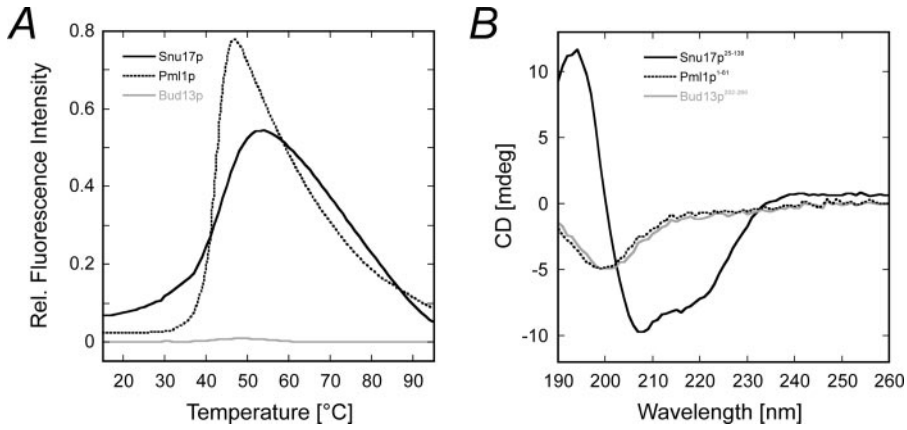

FIGURE 3. **Global fold analysis.** *A*, thermal unfolding of full-length Snu17p (*solid black line*), Pml1p (*dashed line*), and Bud13p (*gray line*) monitored by differential scanning fluorimetry. Snu17p and Pml1p exhibit cooperative transitions, indicative of folded domains. *B*, far-UV CD spectra of Snu17p-(25–138) (*black line*), Pml1p-(1–61) (*dashed line*), and Bud13p-(202–266) (*gray line*) suggest that both the Bud13p and Pml1p portions are disordered in solution. Snu17p-(25–138), which binds both Bud13p and Pml1p, shows a mixed α/β-structure indicated by minima at 208 and 222 nm.

GST-Snu17p fusion protein by *in vitro* pull-down experiments (Fig. 5*B*).

N-terminal truncations of Bud13p, which removed the lysine-rich conserved element, had no influence on binding to GST-Snu17p (Fig. 5*C*, *lanes 20*, *23*, *26*, *29*, *32*, and *35*). In contrast, none of the Bud13p fragments that lacked the C-terminal 65 residues could be precipitated by immobilized GST-Snu17p fusion protein (Fig. 5*C*, *lanes 5*, *8*, *11*, and *14*). The very C-terminal fragment of Bud13p alone (Bud13p-(202–266)) was sufficient to sustain binding to GST-Snu17p (Fig. 5*C*, *lane 35*). These results demonstrate that the Bud13p C terminus encompassing the second highly conserved region is involved in the interaction with Snu17p. In agreement with the fold predictions for Bud13p, equilibrium CD spectra of Bud13p-(202–266) indicated a random coil structure for this part of the protein (Fig. 3*B*).

A Conserved Trp in the C Terminus of Bud13p Is Critical for the Interaction with Snu17p—Among the highly conserved residues at the C terminus of Bud13p, a central Trp (Trp^{232}) stands out (Fig. 5*A*). Similar conserved tryptophans are found in ULMs (Fig. 6*A*), where they are crucial for the interaction with UHMs (19, 24–27). To test the idea that the Bud13p-(202–266) fragment acts like a ULM, using its Trp-containing motif to associate with Snu17p, we mutated Trp^{232} of Bud13p to alanine and analyzed heterodimer formation in mixtures of Snu17p with either an excess of the wild type Bud13p C-terminal fragment (Bud13p-(202–266)) or the mutated fragment (Bud13p-(202–266) (W232A)) by analytical gel filtration. Whereas a stable interaction was observed between wild type Bud13p-(202–266) and Snu17p, the W232A substitution completely abrogated binding of the fragment to Snu17p (Fig. 6*B*). Thus, Trp^{232} of Bud13p represents a critical latching point for interaction with Snu17p, reminiscent of UHM-ULM interactions.

Known UHMs sequester the Trp residue of the bound ULMs in a hydrophobic pocket between their two α-helices. In order to test whether Snu17p positions Trp^{232} of Bud13p in a similar environment, we monitored the intrinsic Trp fluorescence of a chemically synthesized Bud13p peptide encompassing residues 222–242 upon interaction with Snu17p-(25–106) (the latter protein does not contain a Trp). Unbound Bud13p-(222–242) showed an emission maximum at 355 nm, which shifted to 345 nm upon the addition of equimolar amounts of Snu17p-(25–106) (Fig. 6*C*). In addition to the blue shift, the fluorescence quantum yield increased upon complex formation (Fig. 6*C*). These spectral changes are consistent with the transfer of Bud13p Trp^{232} from a polar (aqueous) to a nonpolar (proteinaceous) environment, again supporting a UHM·ULM-type binding mode between Snu17p and Bud13p.

The N Terminus of Pml1p Is Required for Snu17p Binding—To address the question of which part of Pml1p mediates interaction with Snu17p, we engineered various N- and C-terminal truncation mutants of Pml1p (Fig. 7*A*) and tested their binding to recombinant GST-Snu17p in pull-down assays. Some truncations that cut into the predicted C-terminal FHA domain of Pml1p were partially insoluble, suggesting that in these fragments the proper fold of the FHA domain was corrupted. Irrespectively, all polypeptide chains harboring the first 61 amino acid residues were brought down by GST-Snu17p in pull-down assays (Fig. 7*B*, *lanes 5*, *8*, *11*, *14*, *17*, and *20*). These data suggest that the Snu17p-binding capacity of Pml1p does not rely on an intact FHA domain. Since FHA domains often function as phosphopeptide-binding elements (28), the Snu17p-Pml1p interaction is apparently independent of Snu17p phosphorylation. Contrary to the dispensable FHA domain, Pml1p fragments lacking the N-terminal 61 residues failed to interact with Snu17p (Fig. 7*B*, *lanes 26*, *29*, and *32*), and even a deletion of the first 33 residues of Pml1p abrogated the binding (Fig. 7*B*, *lane 23*). Again, disorder predictions suggested that the N-terminal portion of Pml1p is intrinsically unstructured. Equilibrium CD spectra of Pml1p-(1–61) were consistent with a random coil structure in this part of the protein (Fig. 3*B*). Thus, an intrinsically unstructured portion at the N terminus of Pml1p (residues 1–61) is sufficient for interaction with Snu17p, reminiscent of the situation in Bud13p.

Thermodynamic Characterization of Minimal Heterodimers—To test whether the outlined interaction regions of Bud13p and Pml1p contain all Snu17p-contacting elements of the proteins, we compared thermodynamic binding parameters of the full-length and the minimal complexes using ITC. ITC titrations yielded an estimated dissociation constant in the low nanomolar range for the interaction of Snu17p with full-length Bud13p and a value in the low micromolar range for the binding of Snu17p to full-length Pml1p (Fig. 8 and Table 1). Comparable dissociation constants were observed when the shortest interacting fragments of Bud13p (residues 202–266) and Pml1p (residues 1–61) were employed (Table 1). All proteins tested interacted in 1:1 stoichiometries, and the interactions were mainly enthalpically driven. Interaction entropies are large and negative for all protein pairs

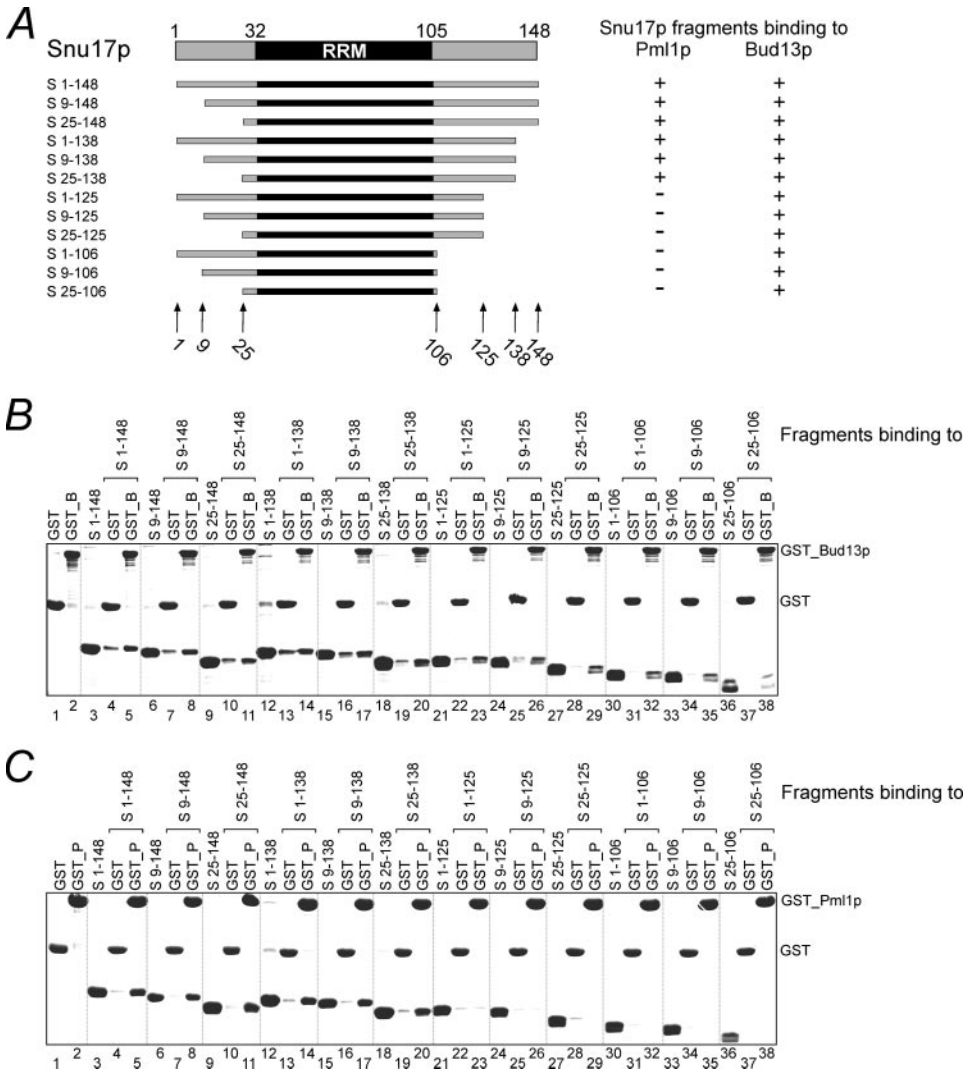

FIGURE 4. **Binding regions of Snu17p for Bud13p and Pml1p.** *A*, schematic representation of Snu17p and of Snu17p fragments engineered for GST pull-down assays. Start and end amino acid residues of the Snu17p fragments are designated on the *left*. Predicted unstructured regions and the central RRM are *colored gray* and *black*, respectively. Interactions of the Snu17p fragments with either Pml1p (*left*) or Bud13p (*right*) are indicated by a *plus sign* (binding) and *minus sign* (no binding) on the *right*. *B*, pull-down of His_6-tagged Snu17p fragments (*A*) with glutathione-Sepharose beads precoated with recombinant GST or GST-Bud13p (GST_B) fusion protein. Input and bound fractions were analyzed by SDS-PAGE. *Lanes 1* and *2*, GST input controls. *Lanes 3*, *6*, *9*, *12*, *15*, *18*, *21*, *24*, *27*, *30*, *33*, and *36*, His_6-tagged inputs used as preys. *Lanes 4*, *7*, *10*, *13*, *16*, *19*, *22*, *25*, *28*, *31*, *34*, and *37*, GST control pull-downs. *Lanes 5*, *8*, *11*, *14*, *17*, *20*, *23*, *26*, *29*, *32*, *35*, and *38*, pull-downs with GST-Bud13p. Snu17p requires only its core RRM to interact with Bud13p. *C*, pull-down of His_6-tagged Snu17p fragments as in *B* but using glutathione-Sepharose beads precoated with recombinant GST or GST-Pml1p (*GST_P*) fusion protein. *S*, Snu17p. Snu17p requires a C-terminal expansion of its core RRM to interact with Pml1p.

(Table 1). Taken together, these data show or corroborate that (i) that Snu17p-binding elements are maintained within the first 61 residues of Pml1p and within the last 65 residues of Bud13p, (ii) both Bud13p and Pml1p employ intrinsically unstructured regions to bind to Snu17p, and (iii) RES components interact stoichiometrically. Furthermore, the particularly strong interaction between Snu17p and Bud13p suggests a permanent association between the two proteins *in vivo*. This notion is supported by the observation that deletions of the two proteins show similar phenotypes in yeast (12, 29, 30). In contrast, the intermediate strength Snu17p-Pml1p complex may be indicative of a transient or facultative, and thus possibly regulated, association.

DISCUSSION

The RES Complex Is Organized around an Unconventional RRM That Binds Multiple Proteins—We have shown that Snu17p is the central subunit of the RES complex, which binds both Bud13p and Pml1p, whereas the latter two proteins do not interact with each other. Bud13p and Pml1p interact with Snu17p exclusively via their C-terminal 65 residues and their N-terminal 61 residues, respectively. Mutational analysis demonstrated that a conserved Trp in Bud13p is essential for complex formation. Structure probing by CD spectroscopy revealed that the interacting portions of both ligand proteins are intrinsically unstructured. Stretches of Bud13p and Pml1p that are immobilized and perhaps locally fold into regular secondary structures upon complex formation could contribute to the large negative binding entropies detected by ITC. However, entropy changes in the solvent, such as desolvation upon complex formation, may well exceed entropic contributions from the solutes. Whether larger portions of the otherwise completely unstructured Bud13p fold upon interaction with Snu17p is presently unclear. Whereas Bud13p binds to the core RRM of Snu17p (residues 25–106), Pml1p requires a C-terminal extension in Snu17p for a stable interaction (residues 25–138).

As further detailed below, these findings show that the Snu17p RRM is unconventional in that it supports two different modes of protein-protein interactions at the same time. On one hand, Snu17p resembles a UHM domain that interacts with a ULM-like motif in Bud13p (19). On the other hand, the binding mode between Snu17p and Pml1p recapitulates features of the complex between the human SF3b14a (p14) protein and a peptide of SF3b155 (20, 21).

The Complex of Snu17p and Bud13p Exhibits Hallmarks of a UHM-ULM Interaction—Compared with canonical RRMs, UHMs exhibit poor conservation of the RNP1 and RNP2 motifs, an Arg-*X*-Phe motif in the loop preceding the core RRM fold, conserved acidic residues in helix A, and a low isoelectric point (the average pI of known UHMs is ~4.5) (19). All UHM-ULM interactions studied in molecular detail exhibited an

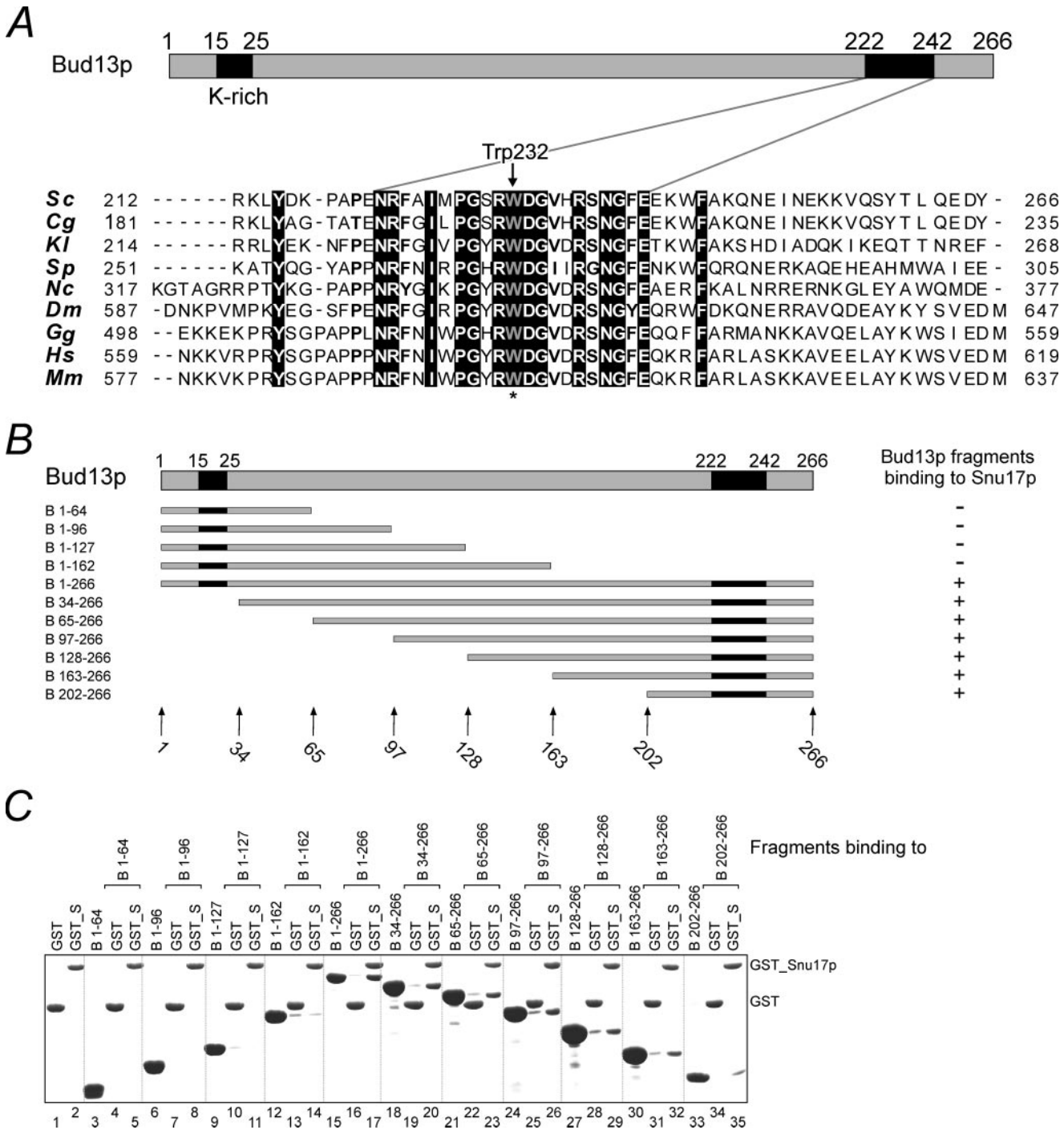

FIGURE 5. **The Snu17p-binding region of Bud13p.** *A* (*top*), schematic representation of Bud13p with conserved regions depicted as *black boxes*. *Bottom*, multiple sequence alignment of the C-terminal region of *S. cerevisiae* (*Sc*) Bud13p with orthologs from *Candida glabrata* (*Cg*), *Kluyveromyces lactis* (*Kl*), *Schizosachharomyces pombe* (*Sp*), *Neurospora crassa* (*Nc*), *Drosophila melanogaster* (*Dm*), *Gallus gallus* (*Gg*), *Homo sapiens* (*Hs*), and *Mus musculus* (*Mm*) shows an Arg-Trp-Asp-Gly motif with a central Trp present in all sequences analyzed. Identical residues are *boxed*. The *numbers* on the *left* and *right* of the alignment indicate the start and end residues of the sequences. The alignment was generated using the ClustalW algorithm (41). *B*, schematic representation of Bud13p fragments engineered for GST pull-down assays with start and end amino acids designated on the *left*. Interactions of the Bud13p fragments with GST-Snu17p (*GST_S*) are indicated by a *plus sign* (binding) and *minus sign* (no binding) on the *right*. *B*, Bud13p. *C*, pull-down of His_6-tagged Bud13p fragments (*A*) with glutathione-Sepharose beads precoated with recombinant GST or GST-Snu17p fusion protein shows that Bud13p binding is dependent on the presence of the C-terminal portion (residues 202–266) harboring the highly conserved C-terminal region. Experimental conditions were as in Fig. 4*B*. *B*, Bud13p.

invariant Trp of the ULM that was inserted into a hydrophobic pocket between helices A and B of the UHM domain. Structure-based mutational analyses demonstrated that this Trp is essential for the interaction in all examples studied (26, 27). In many but not all ULMs, a Ser-Arg dipeptide preceding the invariant Trp is additionally important for the binding to UHMs (24–27). Phosphorylation of the serine residue can modulate the UHM-ULM interaction in some cases. For instance, phosphorylation

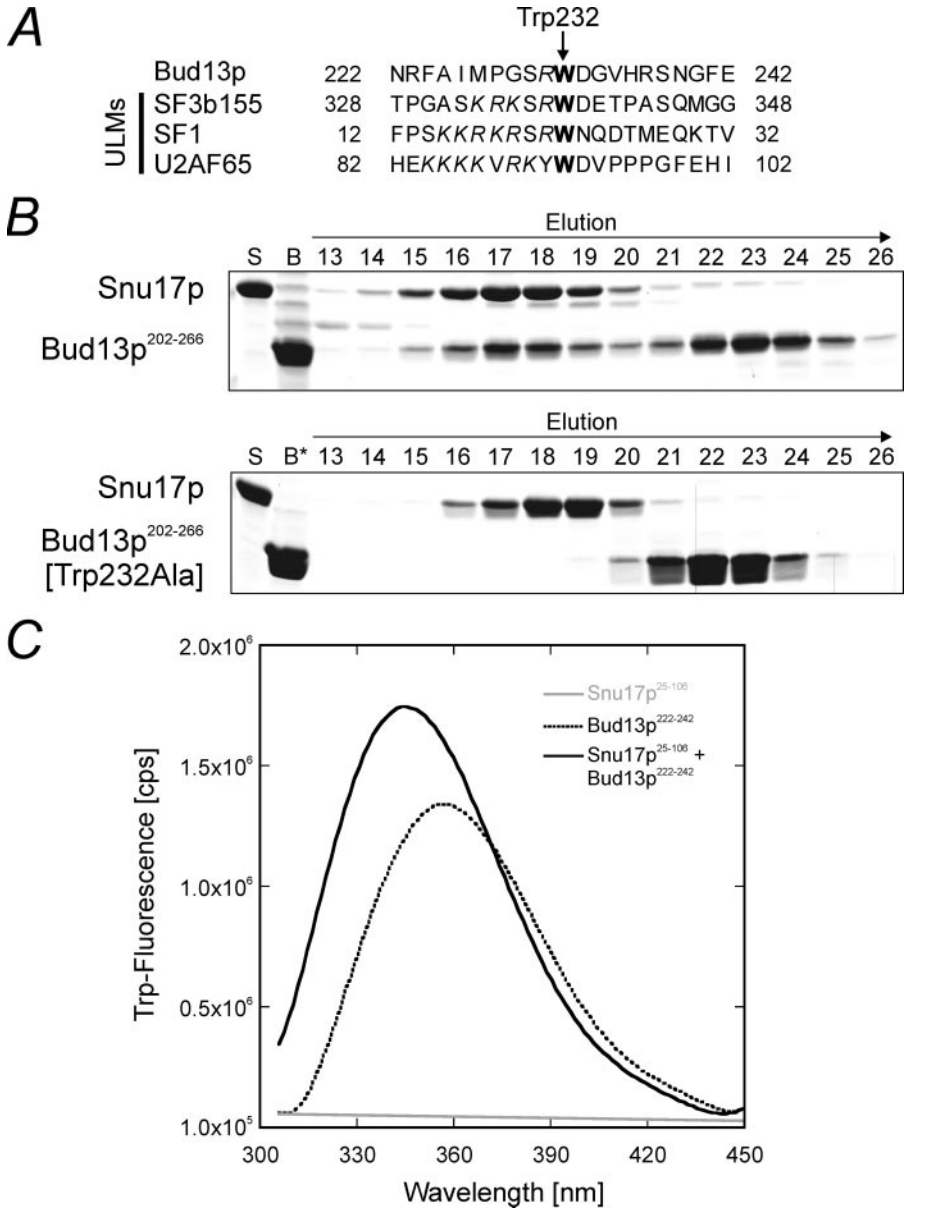

FIGURE 6. **Role of Trp^{232} in Bud13p for binding to Snu17p.** *A*, multiple sequence alignment of the conserved C-terminal portion of Bud13p with ULMs from SF3b-155 (ULM5), SF1, and U2AF65. Trp^{232} of Bud13p and the ULM tryptophans are in *boldface type*, preceding basic residues in *italics*. *B*, gel filtration analysis shows that a dimeric complex forms upon mixing Snu17p and Bud13p-(202–266) fragments (*top*; *fractions 15–20*). In contrast, Bud13p-(202–266) (W232A) does not co-migrate with Snu17p during gel filtration (*bottom*), indicating a crucial role of Trp^{232} in the Snu17p-Bud13p interaction. Protein-containing fractions were analyzed by SDS-PAGE, and proteins were visualized by Coomassie staining. Input controls before mixing are on the *left*. *S*, Snu17p; *B*, Bud13p-(202–266); *B**, Bud13p-(202–266) (W232A). *C*, intrinsic Trp fluorescence emission spectra of unbound Bud13p-(222–242) (*dashed curve*) or bound to Snu17p-(25–106) (*black curve*) suggest burial of Bud13p Trp^{232} in a hydrophobic pocket upon complex formation. Snu17p-(25–106) does not contain Trp (*gray curve*). All spectra were corrected against a buffer spectrum.

of Ser^{20} of SF1 (splicing factor 1) inhibits interaction with U2AF65 and impedes spliceosome assembly (31).

The interaction of Snu17p with Bud13p clearly resembles a UHM-ULM interaction. A W232A mutation in Bud13p completely abolished the interaction with Snu17p. Spectral changes of Trp fluorescence upon complex formation and the high salt stability of the complex suggest that Trp^{232} comes to lie in a hydrophobic pocket upon binding to Snu17p. Furthermore, as observed for UHMs, the core RRM of Snu17p (residues 25–106) is sufficient for binding of Bud13p. In addition, the Snu17p-Bud13p complex exhibits a dissociation constant in the nanomolar range (Table 1), similar to the K_d value determined for the interaction between some other UHM·ULM pairs (*e.g.* the K_d of the U2AF65-U2AF35 interaction is 1.7 nM) (25). Finally, Snu17p exhibits a low pI (5.92).

On the other hand, some other typical UHM sequence characteristics are absent from Snu17p (*e.g.* aromatic amino acid residues of the RNP1 and RNP2 motifs, known to mediate RNA binding in canonical RRMs, are conserved, whereas the UHM-characteristic Arg-*X*-Phe motif is lacking). Therefore, we assume that Snu17p belongs to a new subfamily of RRM-containing proteins, which combine features of RNA-binding RRMs and protein-binding UHMs. An important question for the future is whether Snu17p is also able to interact with RNA.

Ablation of the Snu17p-Bud13p Interaction Has Severe Cellular Consequences—The C-terminal Snu17p-binding portion of Bud13p is the most highly conserved region in the protein, indicating that the interaction between Snu17p and Bud13p is functionally important. In yeast, Bud13p has been identified in a screen for mutants defective in bud site selection (32). Interestingly, deletion of the gene encoding Snu17p was also shown to result in a similar budding defect (32). Furthermore, a Bud13p mutant, encoded by the *slc7-1* allele, showed a synthetic growth defect when combined with a mutant of an essential splicing factor, Clf1 (33). The *slc7-1* allele introduces a nonsense codon into the conserved C-terminal segment of Bud13p at the position of Trp^{232}. Based on our analysis, a mutant Bud13p lacking Trp^{232} will not be able to interact stably with Snu17p. The splicing defect of the *slc7-1* allele and the budding defect of a Bud13p deletion mutant are, therefore, possibly a consequence of impaired pre-mRNA retention or splicing, brought about by the disruption of the Snu17p-Bud13p interaction. Although little is known about the function of Bud13p in other organisms, RNA interference experiments have shown that it is required for *Caenorhabditis elegans* embryogenesis (34). Whether the destruction of the

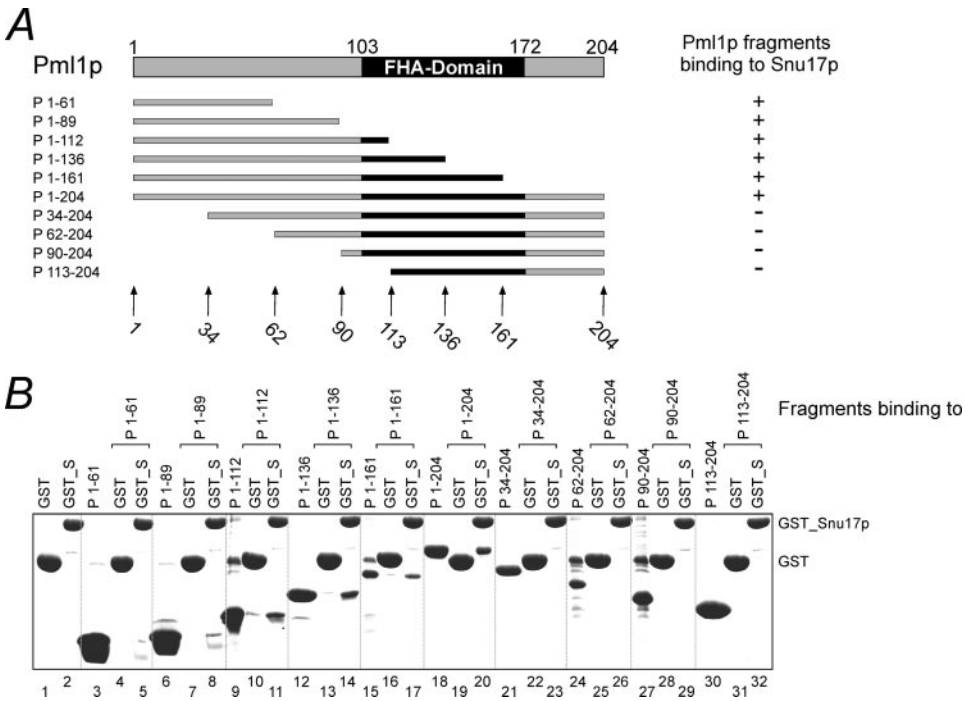

FIGURE 7. **The Snu17p-binding region of Pml1p.** *A*, schematic representation of Pml1p and Pml1p fragments engineered for GST pull-down assays with start and end amino acid residues designated on the *left*. The predicted unstructured N-terminal part of Pml1p is shown in *gray*. The predicted C-terminal FHA domain is shown in *black*. Interactions of the Pml1p fragments with GST-Snu17p fusion protein are indicated by a *plus sign* (binding) and *minus sign* (no binding) on the *right*. *P*, Pml1p. *B*, pull-down of His_6-tagged Pml1p fragments (*A*) with glutathione-Sepharose beads precoated with recombinant GST or GST-Snu17p (*GST_S*) fusion protein shows that Pml1p binding is dependent on the presence of the N-terminal portion (residues 1–33), that residues 1–61 of Pml1p are sufficient for binding to Snu17p, and that the Pml1p FHA-domain is dispensable. Fragments P1–112, P1–161, P62–204, and P90–204 were weakly soluble. *Bands* in *lanes 9*, *15*, *24*, and *27*, which are migrating at the size of GST, are contaminations. Experimental conditions were as in Fig. 4*B*. *P*, Pml1p.

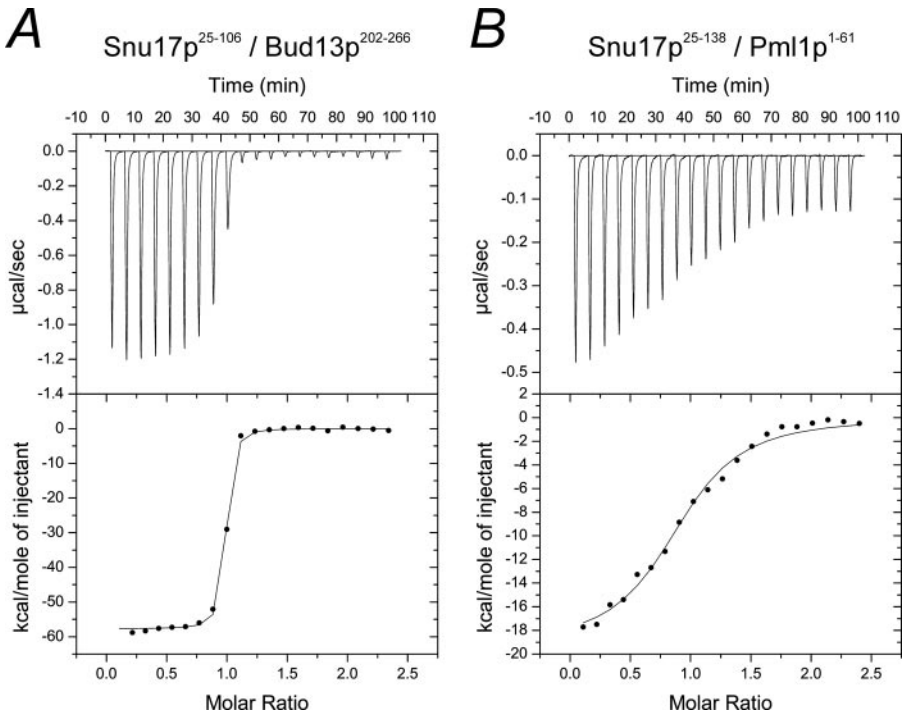

FIGURE 8. **Thermodynamic analyses.** *A* and *B*, representative isothermal titration calorimetry runs for the Snu17p-(25–106)-Bud13p-(202–266) interaction (*A*) and the Snu17p-(25–138)-Pml1p-(1–61) interaction (*B*). Snu17p is capable of binding Bud13p with low nanomolar K_d values, whereas dissociation constants for the Snu17p-Pml1p interactions are in micromolar ranges. All titrations were carried out at 20 °C. The thermodynamic binding parameters are given in Table 1.

Bud13p-Snu17p complex and a consequent defect in pre-mRNA retention or splicing are the main cause for these effects remains to be tested.

The Interaction of Snu17p and Pml1p Resembles the Complex between SF3b14a and SF3b155—A short region beyond the core RRM of Snu17p up to residue 138 is required for stable binding of Pml1p. Previously, a very similar portion of SF3b14a, a suggested Snu17p ortholog in the human SF3b complex, was shown to be required for binding of a peptide of SF3b155 (20, 21). Upon interaction with SF3b14a, the otherwise unstructured SF3b155 peptide adopts a mixed α/β structure (20), reminiscent of the behavior of the N-terminal Snu17p-binding region of Pml1p. SF3b14a and the SF3b155 peptide interact via a stable hydrophobic interface (20). The high salt resistance of the Snu17p-Pml1p complex is also consistent with a strongly hydrophobic interaction mode. Therefore, we suggest that in analogy to the SF3b14a-SF3b155 complex, Snu17p interacts with Pml1p via the surface opposite of helices A and B.

We devised a molecular model in order to visualize how Snu17p could concomitantly bind to the two peptide ligands. The expanded RRM motif of Snu17p was homology-modeled utilizing the Bioinformatics Toolkit server (35) based on the atomic coordinates of the SF3b14a subunit of the SF3b14a-SF3b155 complex crystal structure (20) (Protein Data Bank code 2F9D). We then aligned the SF3b155 fragment and an SF1 ULM peptide from a complex with the C-terminal UHM domain of $U2AF^{65}$ (26) (Protein Data Bank code 1OPI) with the model of the Snu17p RRM (Fig. 9). In our model, the SF3b155 peptide mimics the N-terminal Snu17p-binding portion of Pml1p, whereas the SF1 peptide mimics the C-terminal Snu17p-binding region of Bud13p. In the model, the two ligands come to lie on two neighboring and nonoverlapping interaction surfaces (Fig. 9).

TABLE 1
Isothermal titration calorimetry

Analyte and titrant	K_d	ΔH	ΔS	Stoichiometry
	nM	kcal mol^{-1}	cal K^{-1} mol^{-1}	n
Snu17p-(1–148)				
Bud13p-(1–266)	2.5	−76	−222	1.1
Bud13p-(202–266)	2.6	−61	−170	1.0
Pml1p-(1–204)	1100	−15	−24	0.9
Pml1p-(1–61)	900	−17	−29	0.9
Snu17p-(25–138)				
Pml1p-(1–204)	1000	−16	−28	0.9
Pml1p-(1–61)	600	−19	−37	0.9
Snu17p-(25–106)				
Bud13p-(1–266)	6.8	−53	−143	1.0
Bud13p-(202–266)	5.3	−58	−159	0.9
Bud13p-(202–266) (W232A)	ND[a]			

[a] Not detected.

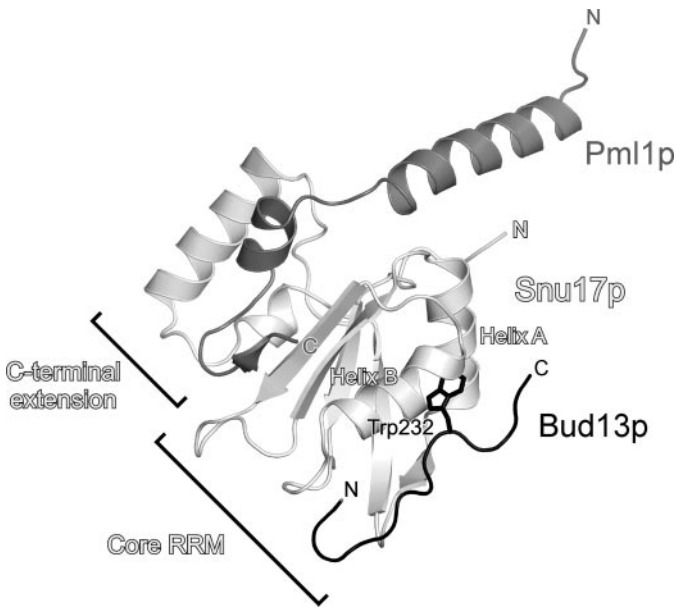

FIGURE 9. **Model of the protein-protein interactions centered on Snu17p.** Snu17p, Pml1p, and Bud13p are shown as *light gray*, *gray*, and *black ribbons*, respectively. Trp^{232} of Bud13p is shown in a *stick representation*. *N*, N termini; *C*, C termini. Helices A and B of Snu17p that sandwich the Bud13p Trp^{232} are labeled. The regions encompassing the core (sufficient to bind Bud13p) and the C-terminal extension of the Snu17p RRM (required to bind Pml1p) are indicated.

Snu17p Displays Functional Elements of Bud13p and Pml1p—Notably, the Snu17p-Bud13p interaction makes use of only a short, conserved region in the C terminus of Bud13p. We suggest that this interaction, therefore, serves to tether other functionally important regions of Bud13p to complexes involved in pre-mRNA retention or splicing. For example, although Bud13p orthologs show considerable length variation, all exhibit a stretch of consecutive Lys or Arg residues in the N termini. Although the role of this region is presently unclear, its conservation clearly points to an important function.

A large C-terminal portion of Pml1p, which is predicted to fold as an FHA domain, is dispensable for the interaction with Snu17p. Recapitulating its mode of interaction with Bud13p, Snu17p binds a short, N-terminal peptide of Pml1p and thereby holds on to a functional motif, the FHA domain, in the ligand protein. It is noteworthy that Snu17p and Pml1p interact with a K_d in the micromolar range (Table 1), significantly higher than the nanomolar K_d of the Snu17p-Bud13p interaction. Therefore, it is possible that Snu17p recruits Pml1p intermittently as a phosphorylation sensor during pre-mRNA retention or splicing.

Linking Pre-mRNA Retention and Splicing via the RES Complex—Presently, the molecular mechanisms, by which unspliced pre-mRNAs are retained in the nucleus, are not well understood (36, 37). Conceivably, a retention factor recognizes portions of the RNAs that mark them as premature transcripts. Snu17p of the RES complex is a candidate for this function. Although we characterized the Snu17p RRM as a protein-binding module, previous examples show that protein interaction does not *a priori* exclude the possibility for concomitant RNA binding by an RRM. For example, although SPF45 constitutes a UHM that forms a complex with a ULM in SF3b155 (24), it additionally interacts with an AG dinucleotide at the 3′-splice site and promotes its utilization for the second catalytic step (38). Similarly, the crystal structure of human SF3b14a with a SF3b155 peptide revealed that although the RRM β-sheet of SF3b14a is largely occluded upon complex formation, the branch site adenosine of pre-mRNA could still be cross-linked to Tyr^{22} of the protein (20). In analogy to these examples, Snu17p could have RNA binding activity and might be specifically targeted to unspliced pre-mRNA molecules in the context of RES.

Interestingly, purine-rich exonic splicing enhancers (*i.e.* sequences in an exon that facilitate regulated splicing in higher eukaryotes) were recently found to support retention of RNAs in the nucleus through a saturable nuclear retention factor (39). Intron-containing pre-mRNAs use the same retention factor as exonic splicing enhancers (39). Perhaps significantly, yeast Snu17p also exhibits splicing enhancer activity (30). Although it remains to be seen whether this function is paralleled by Snu17p orthologs in higher eukaryotes, where regulated splicing takes place, it is conceivable that nuclear retention and splicing enhancement by Snu17p is achieved by binding to the same RNA elements.

Pre-mRNA retention is thought to be mediated by a spliceosome-associated factor (36, 37). Consistently, the RES complex activates splicing (12, 29, 30) and was found in activated precatalytic (14) and step 1 (C complex (16)) spliceosomes in humans. Significantly, Snu17p and Bud13p were found associated with the SF3b complex of yeast U2 snRNP (40), and one human ortholog of Snu17p appears to be the SF3b14a/p14 subunit of SF3b, affording a direct link to the spliceosome. Therefore, one important task for the future will be to delineate the surfaces on the RES complex, through which it is tethered to the spliceosome.

Acknowledgments—We thank Elke Penka for excellent technical support and Katrin Wiederhold and Pavel Burkhardt for help with fluorescence and ITC measurements.

REFERENCES

1. Will, C. L., and Lührmann, R. (2006) *The RNA World*, 3rd Ed., pp. 369–400, Cold Spring Harbor Laboratory, Cold Spring Harbor, NY
2. Jurica, M. S., and Moore, M. J. (2003) *Mol. Cell* **12,** 5–14
3. Nilsen, T. W. (2003) *BioEssays* **25,** 1147–1149

4. Brow, D. A. (2002) *Annu. Rev. Genet.* **36,** 333–360
5. Krämer, A., Gruter, P., Groning, K., and Kastner, B. (1999) *J. Cell Biol.* **145,** 1355–1368
6. Will, C. L., Schneider, C., MacMillan, A. M., Katopodis, N. F., Neubauer, G., Wilm, M., Lührmann, R., and Query, C. C. (2001) *EMBO J.* **20,** 4536–4546
7. Will, C. L., Urlaub, H., Achsel, T., Gentzel, M., Wilm, M., and Lührmann, R. (2002) *EMBO J.* **21,** 4978–4988
8. Ajuh, P., Kuster, B., Panov, K., Zomerdijk, J. C., Mann, M., and Lamond, A. I. (2000) *EMBO J.* **19,** 6569–6581
9. Chen, C. H., Yu, W. C., Tsao, T. Y., Wang, L. Y., Chen, H. R., Lin, J. Y., Tsai, W. Y., and Cheng, S. C. (2002) *Nucleic Acids Res.* **30,** 1029–1037
10. Makarova, O. V., Makarov, E. M., Urlaub, H., Will, C. L., Gentzel, M., Wilm, M., and Lührmann, R. (2004) *EMBO J.* **23,** 2381–2391
11. Tarn, W. Y., Hsu, C. H., Huang, K. T., Chen, H. R., Kao, H. Y., Lee, K. R., and Cheng, S. C. (1994) *EMBO J.* **13,** 2421–2431
12. Dziembowski, A., Ventura, A. P., Rutz, B., Caspary, F., Faux, C., Halgand, F., Laprevote, O., and Seraphin, B. (2004) *EMBO J.* **23,** 4847–4856
13. Behzadnia, N., Golas, M. M., Hartmuth, K., Sander, B., Kastner, B., Deckert, J., Dube, P., Will, C. L., Urlaub, H., Stark, H., and Lührmann, R. (2007) *EMBO J.* **26,** 1737–1748
14. Deckert, J., Hartmuth, K., Boehringer, D., Behzadnia, N., Will, C. L., Kastner, B., Stark, H., Urlaub, H., and Lührmann, R. (2006) *Mol. Cell Biol.* **26,** 5528–5543
15. Gottschalk, A., Bartels, C., Neubauer, G., Lührmann, R., and Fabrizio, P. (2001) *Mol. Cell Biol.* **21,** 3037–3046
16. Bessonov, S., Anokhina, M., Will, C. L., Urlaub, H., and Lührmann, R. (2008) *Nature* **452,** 846–850
17. Antson, A. A. (2000) *Curr. Opin. Struct. Biol.* **10,** 87–94
18. Maris, C., Dominguez, C., and Allain, F. H. (2005) *FEBS J.* **272,** 2118–2131
19. Kielkopf, C. L., Lucke, S., and Green, M. R. (2004) *Genes Dev.* **18,** 1513–1526
20. Schellenberg, M. J., Edwards, R. A., Ritchie, D. B., Kent, O. A., Golas, M. M., Stark, H., Lührmann, R., Glover, J. N., and MacMillan, A. M. (2006) *Proc. Natl. Acad. Sci. U. S. A.* **103,** 1266–1271
21. Spadaccini, R., Reidt, U., Dybkov, O., Will, C., Frank, R., Stier, G., Corsini, L., Wahl, M. C., Lührmann, R., and Sattler, M. (2006) *RNA* **12,** 410–425
22. Vedadi, M., Niesen, F. H., Allali-Hassani, A., Fedorov, O. Y., Finerty, P. J., Jr., Wasney, G. A., Yeung, R., Arrowsmith, C., Ball, L. J., Berglund, H., Hui, R., Marsden, B. D., Nordlund, P., Sundstrom, M., Weigelt, J., and Edwards, A. M. (2006) *Proc. Natl. Acad. Sci. U. S. A.* **103,** 15835–15840
23. Prilusky, J., Felder, C. E., Zeev-Ben-Mordehai, T., Rydberg, E. H., Man, O., Beckmann, J. S., Silman, I., and Sussman, J. L. (2005) *Bioinformatics* **21,** 3435–3438
24. Corsini, L., Bonnal, S., Basquin, J., Hothorn, M., Scheffzek, K., Valcarcel, J., and Sattler, M. (2007) *Nat. Struct. Mol. Biol.* **14,** 620–629
25. Kielkopf, C. L., Rodionova, N. A., Green, M. R., and Burley, S. K. (2001) *Cell* **106,** 595–605
26. Selenko, P., Gregorovic, G., Sprangers, R., Stier, G., Rhani, Z., Kramer, A., and Sattler, M. (2003) *Mol. Cell* **11,** 965–976
27. Thickman, K. R., Swenson, M. C., Kabogo, J. M., Gryczynski, Z., and Kielkopf, C. L. (2006) *J. Mol. Biol.* **356,** 664–683
28. Durocher, D., Henckel, J., Fersht, A. R., and Jackson, S. P. (1999) *Mol. Cell* **4,** 387–394
29. Scherrer, F. W., Jr., and Spingola, M. (2006) *RNA* **12,** 1361–1372
30. Spingola, M., Armisen, J., and Ares, M., Jr. (2004) *Nucleic Acids Res.* **32,** 1242–1250
31. Wang, X., Bruderer, S., Rafi, Z., Xue, J., Milburn, P. J., Kramer, A., and Robinson, P. J. (1999) *EMBO J.* **18,** 4549–4559
32. Ni, L., and Snyder, M. (2001) *Mol. Biol. Cell* **12,** 2147–2170
33. Vincent, K., Wang, Q., Jay, S., Hobbs, K., and Rymond, B. C. (2003) *Genetics* **164,** 895–907
34. Jiang, M., Ryu, J., Kiraly, M., Duke, K., Reinke, V., and Kim, S. K. (2001) *Proc. Natl. Acad. Sci. U. S. A.* **98,** 218–223
35. Soding, J., Biegert, A., and Lupas, A. N. (2005) *Nucleic Acids Res.* **33,** W244–248
36. Saguez, C., Olesen, J. R., and Jensen, T. H. (2005) *Curr. Opin. Cell Biol.* **17,** 287–293
37. Sommer, P., and Nehrbass, U. (2005) *Curr. Opin. Cell Biol.* **17,** 294–301
38. Lallena, M. J., Chalmers, K. J., Llamazares, S., Lamond, A. I., and Valcarcel, J. (2002) *Cell* **109,** 285–296
39. Taniguchi, I., Masuyama, K., and Ohno, M. (2007) *Proc. Natl. Acad. Sci. U. S. A.* **104,** 13684–13689
40. Wang, Q., He, J., Lynn, B., and Rymond, B. C. (2005) *Mol. Cell Biol.* **25,** 10745–10754
41. Thompson, J. D., Higgins, D. G., and Gibson, T. J. (1994) *Nucleic Acids Res.* **22,** 4673–4680